Article

Not peer-reviewed version

Characterization of the Laser Textured Surfaces of Parts from Arbofill Fichte

Petronela-Daniela Rusu (Ostahie) , Oktawian Bialas , Anna Wozniak , Marcin Adamiak , Catalin Tampu , Simona-Nicoleta Mazurchevici , Teodor-Daniel Mindru , Dumitru Nedelcu *

Posted Date: 11 December 2024

doi: 10.20944/preprints202412.0943.v1

Keywords: Arbofill Fichte; surface texturing; WCA; friction coefficient; wear track

Article

Characterization of the Laser Textured Surfaces of Parts from Arbofill Fichte

Petronela-Daniela Rusu (Ostahie) [1], Oktawian Bialas [2], Anna Wozniak [2], Marcin Adamiak [2], Catalin Tampu [3], Simona-Nicoleta Mazurchevici [1], Daniel Mindru [1] and Dumitru Nedelcu [1,*]

[1] Gheorghe Asachi Technical University of Iasi
[2] Silesian University of Technology
[3] Vasile Alecsandri University of Bacau
* Correspondence: dumitru.nedelcu@academic.tuiasi.ro; Tel.: +040771346968

Abstract: Surface texturing entails surface alteration through forming, micro grooving, micro dimpling and microchanneling. This is achieved by laser micromachining, in addition to other related methods on the substrate surface. The present paper puts forward the surface characteristics obtained after the laser texturing of the Arbofill Fichte biodegradable polymers with four and six passes, in hex-agonal and square patterns. The results of the wettability test indicated that Arbofill Fichte has a surface with a weak hydrophobic character (contact angle near 90°), regardless of the type of texture that was obtained. The underlying material's wear behaviour changed as a result of the Laser Surface Texturing (LST) surface alteration. Friction coefficient (COF) values thus increased for all samples. Arbofill Fichte exhibits a higher Y-axis stability in both geometries, suggesting a better resistance to vertical compression (subsidence), particularly in the 6 passes case. Additionally, Arbofill Fichte has a better X-axis extension. Therefore, Arbofill Fichte is stable and uniform in both geometries and at both numbers of passes, providing a more consistent X-axis expansion and better-managed Y-axis compression. The possibility of use in the practice of textured surfaces is viable; thus, based on the obtained results, there is even the possibility to replace non-biodegradable polymers from different sectors of activity.

Keywords: Arbofill Fichte; surface texturing; WCA; friction coefficient; wear track

---

1. Introduction

Creating the desired pattern on a surface can be accomplished through the use of a process known as surface texturing. Increasing fatigue strength, corrosion resistance, wear resistance, anti-biofouling hydrophobicity and load-carrying capacity are just few of the mechanical and tribological features that make significant use of this material. Several technical materials, including ceramics [1,2], metals [3,4], and polymers [5], have been successfully treated with Laser Surface Texturing (LST). This approach has been effective in a number of technical fields, including coatings, tribology and biomedicine. LST has produced a variety of patterns and textures to improve the material's tribological behaviour. Furthermore, the procedure improves the material's wear resistance and coefficient of friction. A few of the patterns are different sized and shaped dimples and microgrooves [6–8].

Polymers and biopolymers, as natural or artificial ones, have a widespread application in the field of biomedical applications, [9], because of their biocompatibility and good mechanical properties which, in some cases, can be similar to those found in human tissues, [10]. The application of three different laser wavelengths (1.064 µm, 532 nm, and 355 nm) to the carbon-coated surface of polyethylene (UHMWPE) materials and the examination of the impact of laser parameters on the material's surface properties show that the 355 nm and 532 nm wavelength laser is comparatively suitable for improving the surface conditions of UHMWPE, including surface roughness and wettability. With significant changes to the treated polymer surface's mechanical properties, CO_2

laser texturing of poly-l-lactide offers the capacity to modify the material's surface structural and physical properties to the requirements of the cells, [11]. Using 1.064 µm, 355 nm, and 532 nm lasers, the effects of laser variation on the wettability, roughness, and hardness of polypropylene material were investigated. The authors proposed that polypropylene's surface should be roughened with laser wavelengths [12]. According to the scientific literature, Ra values greater than 1 µm are a minimum necessary value to improve bone bonding on the implant surface. By grafting to the polymer with a pulsed CO_2 laser at different laser powers, Mirzadeh et al. [43] enhanced the hydrophilicity and biocompatibility of ethylene-propylene rubber N-vinylpyrrolidone (NVP) and 2-hydroxyethyl methacrylate (HEMA). Dinca V et al. [13] used excimer lasers to conduct single-step creation experiments for roughness gradients on natural composite substrates. According to Koufaki et al.'s [44] investigation into the possibility of cell adhesion on high rough polymeric surfaces with gradient roughness ratio and wettability created by laser micro/nano-textured Si surfaces, both cell types adhered to microstructured surfaces linked to unstructured surfaces more successfully. Moreover, it was shown that PC12 cells adhered well to the patterned surface, [14]. After four days, when the cells multiplied into a merging patch inside the channels, direct laser writing on the biodegradable polymer to create microchannels for the attachment of C_2C_{12} myoblast cells in the microchannels shows a high degree of alignment, [15]. The surface characteristics and properties of nylon 6,6 treated with a CO_2 laser were given by Waugh et al., [16]. They proposed that the biomimetic properties of nylon 6,6 in terms of osteoblast cell response are enhanced by laser textured surfaces.

Few polymeric biomaterials are being utilized in clinical practice today, despite the fact that many have been investigated for tissue engineering [17–19], as follows:

- Poly(Etheretherketone) (PEEK): has excellent mechanical properties (in some cases, even similar to cortical bone), high chemical resistant and exhibits sterilization capacity. So far, surface functionalization of PEEK by means of LST has been successfully achieved using laser wavelengths ranging from UV (355 nm) to middle infrared (MIR) (10.6 µm). PEEK was observed to respond very differently as a function of the laser radiation. The 1,064 nm laser radiation burned the surface, while the 532 nm laser radiation was able to ablate the material. Using this laser wavelength, grooves with a mean width of 100 µm were machined. The 355 nm laser radiation only produced a slight surface melting; however, this laser radiation was identified as the most suitable for biomedical purposes because induced the formation of some polar groups. The main applications are in orthopedic applications (e.g., in joint replacement, cage implants, bone screws, and pins, etc.) [20–25].

- Polypropylene (PP): has good biostability, good thermal stability, and appropriate mechanical properties. However, PP exhibits low surface energy, which hinders its systematic use for tissue replacement [26,27]. The effect of treatment under 1,064, 532, and 355 nm laser wavelengths on the surface features of PP was evaluated [12]. A layer of carbon black was used to increase the original absorption features of this thermoplastic given its high transmittance for wavelengths ranging between 400 and 1,600 nm [28]. The treated surfaces were characterized in terms of surface roughness (Ra), WCA, microhardness, and chemical composition in the treated surfaces. LST of PP resulted in the melting of the surface, along with the adhesion of carbon particles on its surface. The final roughness (Ra) was found to be higher than 1 µm, which is considered the minimum required value to improve the bone/implant bonding degree [29]. Murahara and Okoshi [30] followed a different approach to increase the wettability of PP. This material was irradiated in the presence of tap water by a laser beam produced by an ArF laser. The measurement of the contact angle showed a minimum (contact angle for base material: 93°, and minimum angle for the laser treated surfaces 65°) for a certain fluence and shot number (laser fluence of 12.5 mJ/cm^2 and a shot number of 10,000) [30].

- Polyethylene (PE): PE is a synthetic thermoplastic polymer, bioinert, and non-biodegradable in contact with corporal fluids. LST has been applied to this material given to its inertness [31–34]. Okoshi and Inoue [32] studied the utilization of fs laser sources to ablate and modify the surface of PE samples. LST on PE was performed with a fs Ti:Sapphire laser source using 790 nm laser light, and second harmonics 395 nm. Both wavelengths were found to successfully ablate PE surfaces [32,34]. The biological performance of PE laser textured surfaces was evaluated after being subjected to Nd:YAG laser radiation (λ = 1,064 nm) by Blanchemain et al. [33]. After laser irradiation, the surface roughness of PE was increased up to a value of Ra = 0.2 μm [33]. Among the typical implant applications of this material, chin, cheek, and jaw reconstruction should be highlighted [31–38].

- Polyimide (PI): was textured using different laser wavelengths (λ = 1,064, 532, 355, and 266 nm) to avoid the biofilm formation on indwelling medical devices. Several topographies were tested against Staphylococcus aureus adhesion [39].

Many medical equipments benefit from textured surfaces. Therefore, Yasaka K. et al. [40] studied how textured surfaces affect plastic materials to reduce friction between biological tissues and medical device components. It was found that textured soft plastic surfaces had less friction than conventional surfaces. Ikeuchi K. et al. [41] examined water-based polyurethane grafted with DMAA's tribology. Painless insertion, precision functioning and tissue protection are possible using DMAA-coated medical devices.

Shivakoti et al. [42] postulates that LST shows great biomedical promise, especially for polymers. Mirzadeh et al. [43] used a pulsed CO_2 laser at varying intensities to graft N-vinylpyrrolidone (NVP) and 2-hydroxyethyl methacrylate (HEMA) onto ethylene-propylene rubber to improve its hydrophilicity and biocompatibility. On untreated films, alveolar macrophages adhere to cells and propagate and flatten, while those on treated EPR have a circular shape with limited cytoplasmic spreading and ruffling.

Both cell types adhered better to microstructured surfaces than unstructured surfaces, especially high-roughness polymeric surfaces with gradient roughness ratios and wettability generated by laser micro/nano-textured silicon surfaces, according to Koufaki et al. [44]. It was also showed that PC12 cells attached well to the patterned surface. Evangelista et al. [45] state that current equipment needs modifications to improve medical device tribological qualities while retaining its core features and design.

Surface interactions, or tribology, can influence medical device operation. Prosthetic implants, artificial joints and dynamic mechanisms in drug delivery systems have higher failure rates due to wear and friction than devices without relative motion [46–48].

Using laser texturing, Biala et al. [49] investigated the feasibility of obtaining surface-infused nano gold particles using PEEK.

The desired aim and objective from a scientific point of view is as follows: the study of Arbofill Fichte material with textured surface in order to recommend it in different medical applications. The practical novelty of this study consists in characterization of this biomaterial after applying the surface treatment using LST. This material, treated with LST, did not represent a particular focus point of scientific research. So, the texturing of the surfaces was done with 4 and 6 passes for the parts obtained by injection moulding, hexagonal and square geometries and characterization of the obtained sample. The mechanical, thermal and structural properties of the mentioned materials were studied by the researchers in the papers [50–54].

2.1. Samples Preparation

The biopolymer Arbofill Fichte which was patented by a group of researchers from the Fraunhofer Institute for Chemical Technology (ICT) in Pfinztal, Germany, in association with the business Tecnaro GmbH, has the potential to be used in a wide range of industrial applications, including those involving renewable resources and biopolymers such as polyester (e.g., bio-PET), polyhydroxyalkanoates (PHAs), poly-caprolactone (PCL), starch, polylactic acid (PLA), bio-polyolefins (bio-PEs), bio-polyamides (bio-PAs), lignin, natural resins, natural waxes, natural oils, natural fatty acids, cellulose, organic additives, and natural reinforcing fibres [55]. The main characteristics of Arbofill Fichte according to some previously study realized by a part of research team are: melt volume rate 6cm^3/10min; heat deflection temperature 111°C; impact strength 17KJ/m^2, [54,55]; tensile strength sample as 28 MPa at room temperature (RT), 13.5 MPa at 60°C, tensile strain at fracture of 4.71% (at RT) and 7.1% (60°C), [53]. relative density 1.08, microhardness in the range 0.07804 MPa [56]. Furthermore, a dry friction coefficient in the range 0.145–0.15 has been reported for pin against AISI 572 Gr 65 (OL60) steel disk [53]. The samples used for texturing were obtained by injection moulding using the SZ-600H injection machine (Shen Zhou, Zhangjiagang, China). To obtain better quality results, homogenized sample preparation was used for each sample. Before laser micromachining, the mechanical finishing process was performed using the grinding–polishing machine, known as TERGAMIN-30 (Struers, Willich, Germany). Each sample was mechanically planed and sequentially polished with paper grain-size gradations of 500, 800, and 1200 grid/mm^2 in time t = 4 min per each gradient, and mechanically polished by polishing wheels, with gradations of 9, 3, and 1 μm.

2.2. Laser Surface Texturing (LST)

The surface texturing process utilized an A-355 picosecond laser system (Oxford Lasers Ltd, Didcot, UK), featuring a 335 nm wavelength diode-pumped solid-state picosecond laser. This system generates 5-10 ps pulse durations with 120 μJ energy at a pulse frequency of 400 Hz. The average laser power for the texturing system was 24 mW, with a Gaussian distribution of laser beam intensity. The laser pattern (or filling strategy) was designed with the Cimita software (Oxford Lasers, Didcot, UK) integrated into the micromachining system.

The LST process was given the following parameters presented in Table 1.

Table 1. LST process parameters**.**

Software	Cimita laser micromachining software suite for laser, motion, and vision
Laser	Diode-pumped solid state
Cut speed	1 [mm/s]
Cut passes	4 and 6 passes
Power	48 [mW]
Pulsation frequency	400 [Hz]
Wave length	355 [nm]
Pulse width	6 [ps]

2.2.1. Microscopic Observation

The geometric structure of the sample's surfaces and the wear tracks were analyzed using a Leica DVM6 digital microscope (DM).

2.2.2. Wettability Test

Contact angle (Θ) measurements were carried out using the sitting drop method to determine the wettability of the tested samples surface. For this purpose, the Biolin Scientific Attension Theta Flex strain gauge was used. Drops of distilled water as measuring liquid in the volume of 2 μl were deposited on the surface of the tested samples, each time maintaining the minimum (same) height of the dispenser above the surface. Contact angle measurements were performed as a function of time (60 s) in a series of 3 measurements for each sample. Measurements were carried out at room temperature 289 K (25°C).

2.2.3. Wear Test

The tribological properties of the tested samples were investigated using the ball-on-plate method using a CSM tribometer (CSM Instruments, Needham, MA USA). As a counter sample, an Al_2O_3 ceramic ball with a 6 mm diameter was used. Normal loads of 4 N were used. The stroke length was fixed at 6 mm and the frequency was 1 Hz creating a sliding speed of 1.2 cm/s.

2.2.4. Scanning Electron Microscopy (SEM)

Scanning electron microscopy (SEM) was carried out using a QUANTA 200 3D SEM-FIB electron microscope (FEI Company, Fremont, CA, USA). The following parameters were used: the secondary electrons' acceleration voltage—30 KV; 100X-5000X magnification power; working distance—15 mm; (large field detector (LFD); tilt angle of 0◦, and the pressure of the microscope chamber—60 Pa.

2.2.5. Degradation Test

Degradation test was performed using WKL 100/40 - Weiss Climate chamber according to PN-EN 600068-14 standard. The test parameters are as follows:

- T↓ - T=-5°C w t = 1 h
- Aging: T= -5°C. t= 3 h
- T↑ - T= 50°C. HD = 90%. t =1 h
- Aging – T = 50°C. HD = 90%. t =3 h

The surface morphology after degradation test of the sample's surfaces and the wear tracks were analyzed using a Leica DVM6 digital microscope (DM).

2.2.6. Topography

The Zegage type profilometer was used to determine the topography of the surface. This is an advanced measuring equipment used to analyze the topography of surfaces at a micrometric or nanometric scale, providing an accurate assessment of roughness and other surface characteristics. The Zegage Pro profilometer uses non-contact optical measurement technology based on short coherence interferometry to capture the topography of surfaces at high resolution. This method allows accurate measurements without damaging or altering the surface of the samples. Considering the small roughness values on the measured surface for the determinations, an eyepiece with a magnification of 10 X was used. It has a field of view (FOV- Field of view) of 0.83/0.83 mm and a lateral resolution of 0.815 microns. Lateral resolution means that the profilometer is able to distinguish two points at a minimum distance of 0.815 microns from each other on the measured surface. In other words, two surface details that are separated by a distance greater than or equal to 0.815 microns will appear as distinct in the profilometer image.

3. Results and Discussion

3.1. Microscopic Observation

The surface morphology of the samples after the laser texturing process is shown in Figures 1 and 2. For all of the tested samples, regardless of the type of the base materials groups, honeycomb (group H), and cross-like micro-groove (group S) patterns were observed, which are characteristic features of photothermal ablation. In this sense, transverse and parallel cuts demonstrated the wavy profile which constitutes the texture. The diameter of the dimples was very even and fitted the design well. Based on the microscopic investigation it can be found that grooves present typical laser-induced surface structures, which were formed by the interaction of the laser beam and the sample surface. The textured surfaces obtained by laser ablation have been characterized as continuous grooves, characterized by a regular explosively evaporated bottom.

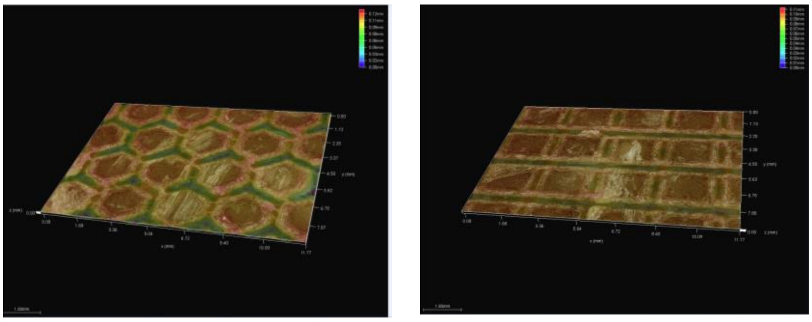
(a) (b)

Figure 1. Microscopic observation of Arbofill Fichte after laser texturing process (a) 4x_H x300, (b) 4x_S x300.

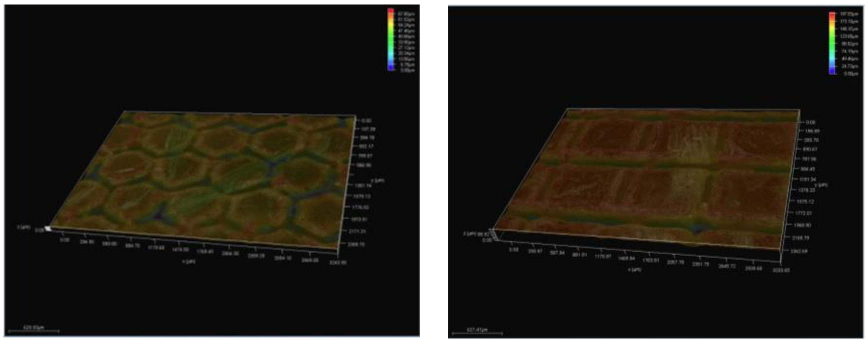
(a) (b)

Figure 2. Microscopic observation of Arbofill Fichte after laser texturing process (a) 6x_H x300, (b) 6x_S x300.

3.2. Wettability Test

The mean value of the distilled water wetting angle for the samples in the initial state was 87±3°, Figure 3, indicating the weak hydrophobic character of the surface (the contact angle close to 90°). Surface modification by laser texturing altered the chemical character of the samples' surface. In case of four texturing passes (4x) and H texture pattern samples group, lower value of water contact angle was recorded and the mean value was close to 38±2° (hydrophilic character of the surface) (Figure 4b). However, for the experiment with 4x and S texture pattern samples group, the initial (maximum) value of the contact angle was close to 19°, and after approximately 16 seconds, the value reached 0° (Figure 4b). It can be noted that the samples exhibited superhydrophilic properties after the initial wetting of the surface (Figure 4a), (Table 2). For the experiment with six texturing passes (6x) samples group, regardless of the texture pattern, similar character of the surface was observed. However, regardless of the texture pattern (S or H) the time after which the contact angle was 0° was different: experiment with 4x and H texture pattern samples group – 15s (Figure 5b), and experiment with 6x and S texture pattern samples group– 1s (Figure 5a). The experiment with 6x and S texture pattern samples group exhibited absolute hydrophilic properties.

Table 2. Contact angle for Arbofill Fichte.

Arbofill Fichte		Arbofill Fichte 4 texturing passes						Arbofill Fichte 6 texturing passes				
No of samples	Contact angle (°)	Texturing type	No of samples	Contact angle (°)				Texturing type	No of samples	Contact angle (°)		
				Max.	Min.	Average				Max.	Min.	Average
1	89	Hexagon	1	-	-	41	38±2	Hexagon	1	40	0 (22s)	-
2	84		2	-	-	35			2	20	0 (9s)	-
3	90		3	-	-	37			3	35	0 (15s)	-
Average	87±3	Square	1	24	0 (15s)	-		Square	1	14	0 (2s)	-
			2	16	0 (20s)	-			2	18	0 (2s)	-
			3	18	0 (15s)	-			3	15	0 (1s)	-

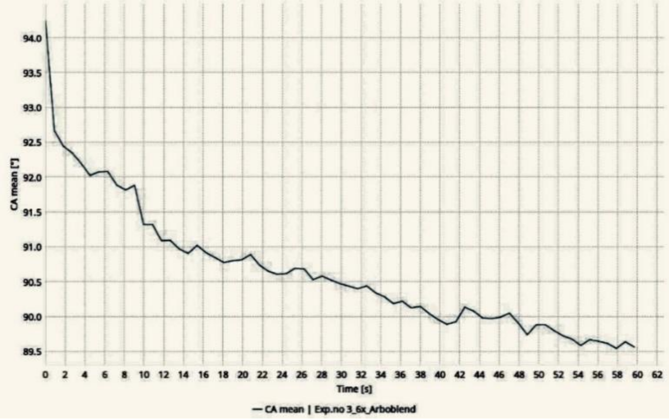

Figure 3. Contact angle diagram for Arbofill Fichte in initial state**.**

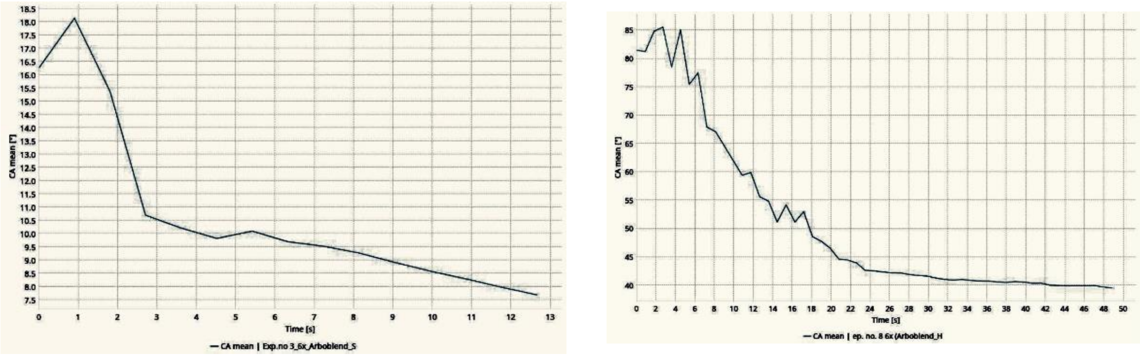

(a) (b)

Figure 4. Contact angle diagram for the experiment with 4x (Arbofill Fichte): (a) S, (b) H**.**

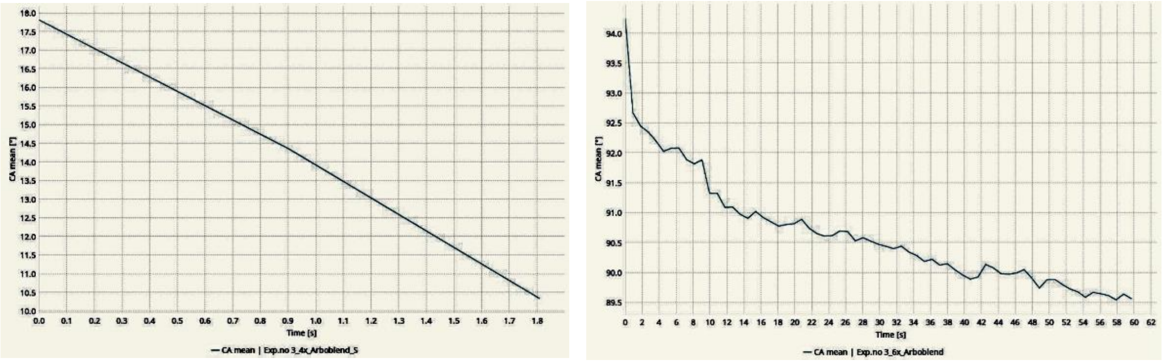

(a) (b)

Figure 5. Contact angle diagram for the experiment with 6x (Arbofill Fichte): (a) S, (b) H**.**

3.3. Wear Test

Table 3 shows the results of the coefficients of friction for both materials studied including the coefficients of friction for both materials before texturing.

Table 3. COF values.

Arbofill Fichte – COF 0.10 initial state		COF
4 texturing passes	Hexagon	0.20
	Square	0.51

6 texturing passes	Hexagon	0.26
	Square	0.49

The mean value of the coefficient of friction (COF) for the Arbofill Fichte samples group in the initial state was 0.10 (Figure 6a). For this sample group, the COF initially decreased during the wear resistance test, likely due to the presence of roughness on both surfaces (tested samples and Al_2O_3 ball - counter specimen) in contact. The point contact between the tested samples and the ceramic ball results in high local compressive pressure, leading to elevated shear stress. Consequently, the surfaces underwent sequential deformation and fragmentation, accelerating wear and representing a typical sliding wear mechanism. Subsequently, the contact area increased over time along with the roughness of the frictional couple's surfaces, resulting in reduced pressure and gradual deceleration.

Surface modification by laser texturing induced a change in the wear behavior of the base material. For all tested samples after the laser texturing process, regardless of both the process parameters and texture pattern, an increase in the COF value was recorded. For samples with an H-texture pattern, the COF value increase at 0.26 in case of 6 passes. However, for samples with an S-texture pattern, an increase in the COF value was observed, with the value of 0.51 for 4 passes. Additionally, for this sample group, the COF value increased in the initial stages of the wear resistance test, Figure 7a, from 0.15 to 0.5, suggesting the removal of the texture pattern during the wear test, as confirmed by microscopic observation (Figure 7b-e). It was found that, for all samples after the laser texturing process, the textured pattern was indeed removed during the wear test under the proposed conditions.

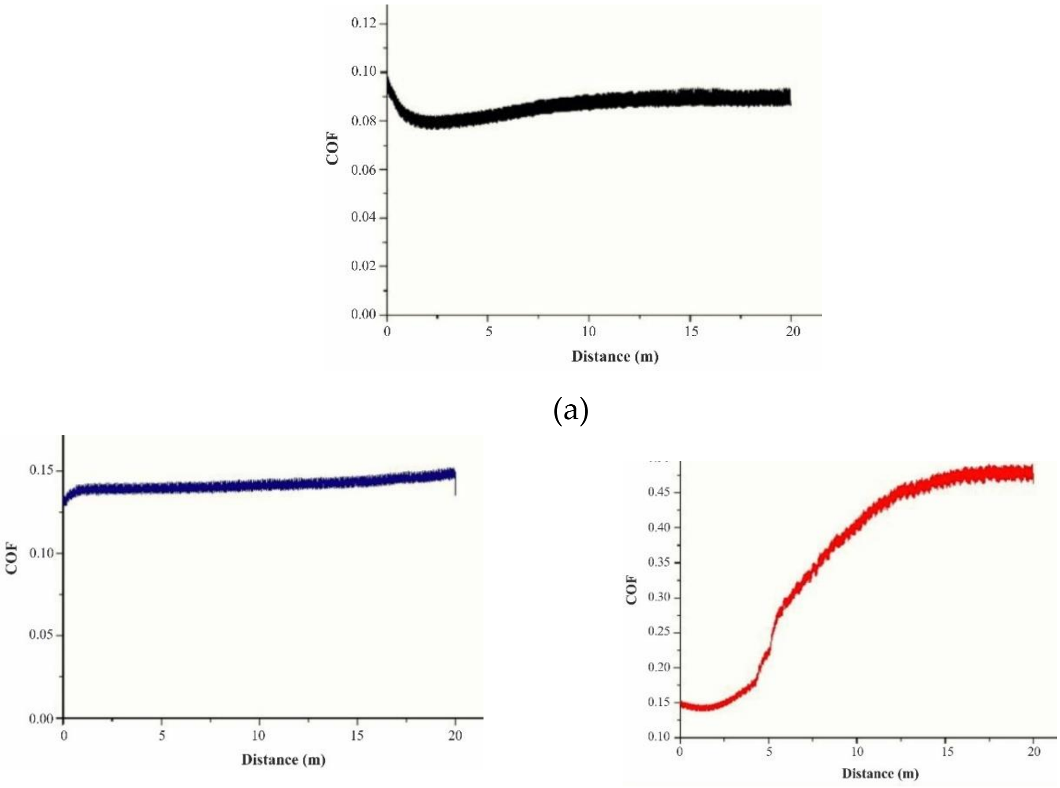

(a)

(b)

(c)

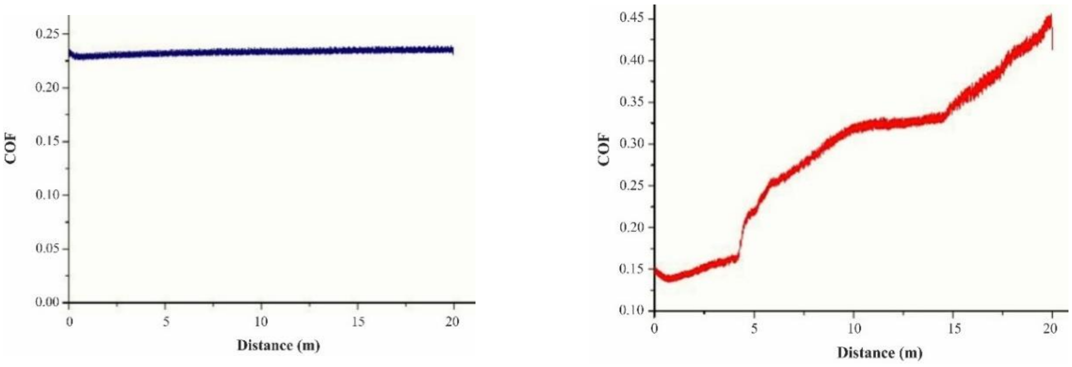

(d)

(e)

Figure 6. Results of COF tests for Arbofill Fichte: (a) base material, (b) 4x_H, (c) 4x S, (d) 6x_H, (e) 6x_S.

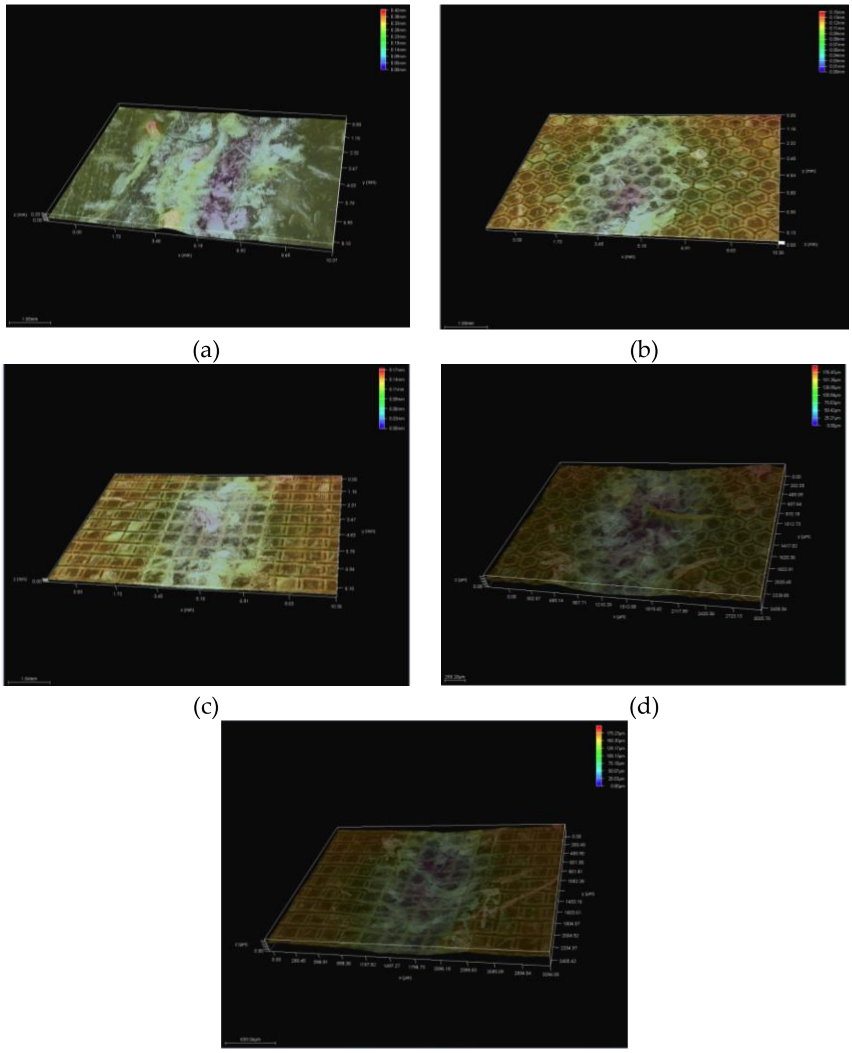

(a)

(b)

(c)

(d)

(e)

Figure 7. Wear track morphology of Arbofill Fichte samples group: (a) base material x100; (b) 4x_H x100; (c) 4x_S x100; (d) 6x_H x100; (e) 6x_S x100.

3.4. Degradation Test

Based on the obtained results of weight measurements before and after the degradation test, an increase in weight was observed for all tested samples, 0.036g in case of 4 passes and 0.039 in case of

6 texturing passes,Table 4. Generally, an increase in weight of polymer materials after a degradation test could indicate incomplete degradation; if the degradation process is not fully completed, residues from partially degraded polymer molecules may remain, contributing to the weight increase. However, based on the microscopic observation of all samples after the degradation test (Figures 8–10), no degradation products were visible. Interaction polymer-based materials with the testing environment (exposure to degradation conditions) might cause chemical reactions that result in weight gain. In some cases, degradation processes can result in cross-linking of polymer chains, which can also increase the weight of the material.

Table 4. Results of degradation test**.**

Material		Weight (g)		Difference
		Before texturing	After texturing	
Arbofill Fichte	4 texturing passes	30.123	30.159	+0.036
	6 texturing passes	31.697	31.736	+0.039

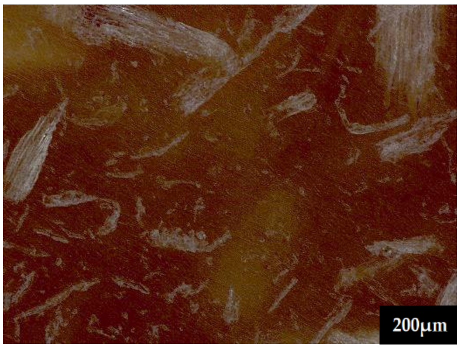

Figure 8. Microscopic observation of laser textured Arbofill Fichte in initial state after degradation test**.**

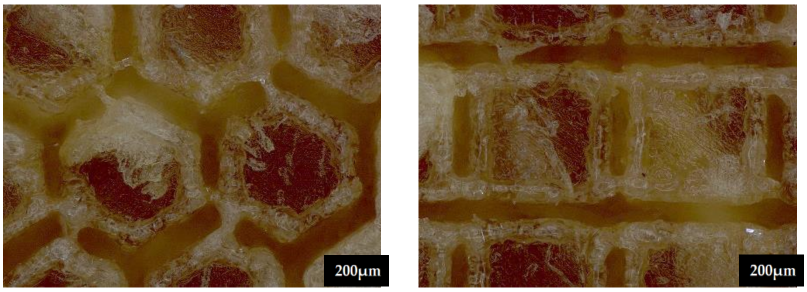

(a) (b)

Figure 9. Microscopic observation of laser textured Arbofill Fichte after degradation test: (a) and (b) 4x_H; (c) and (d) 4x_S.

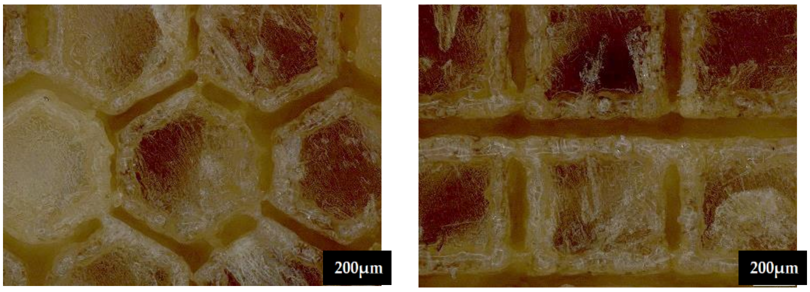

(a) (b)

Figure 10. Microscopic observation of laser textured Arbofill Fichte after degradation test: (a) 6x_H; (b) 4x_S.

3.5. Topography

3.5.1. Topographic Analysis of Arbofill Fichte with Hexagonal Texture

In the case of the Arbofill Fichte material with hexagonal texture obtained by 4 passes, the largest distance between the lowest and the highest peak (PV_Peak and Valley) for the three sections considered is shown in Figure 11, and in Table 5 the corresponding statistical data are presented. Root Mean Square (RMS) has the highest value (10.22 μm) for the slice 2 while the PV maxim value of 64.88 μm was in case of slice 3. Figure 12 displays the flatness deviation following texturing, which, according to ISO Flatness, is 10.848 μm. The roughness values Ra for the three selected reference lines are displayed in Figure 13, and they only match the hexagonal surfaces that were created without accounting for the spacing between hexagons. With the greatest values of Ra=12.145 μm (slice 1) and PV=24.221 μm in the case of slice 3, the resulting Sa value was 8.778 μm.

Table 5. Statistical data for Arbofill Fichte: 4x_H.

Nr.crt.	Reference line	PV (μm)	RMS (μm)
1	Slice 1	34.28	8.67
2	Slice 2	46.68	10.22
3	Slice 3	64.88	9.24
4	Mean	48.61	9.38
5	Standard deviation	15.38	0.78
6	Range	30.59	1.58
7	3 Sigma	46.16	2.35

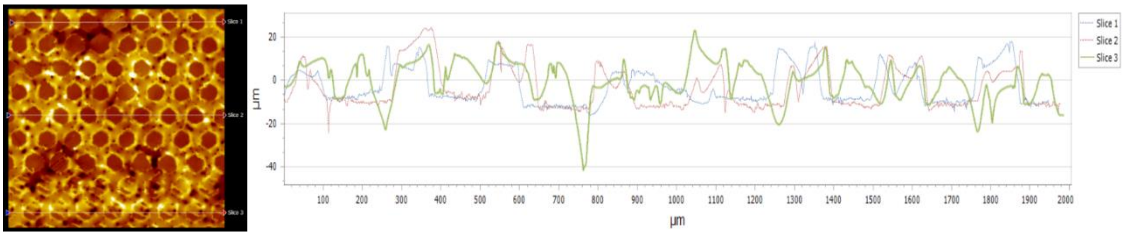

Figure 11. Maximum PV value from the analysis of the three sections - Arbofill Fichte: 4x_H, on the geometric shape.

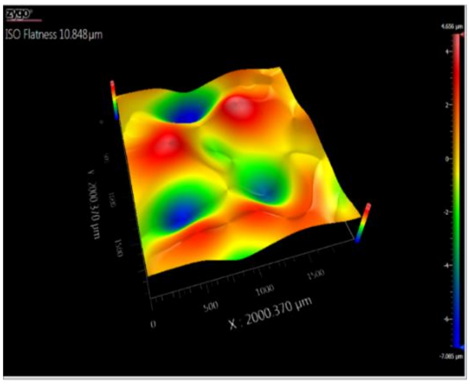

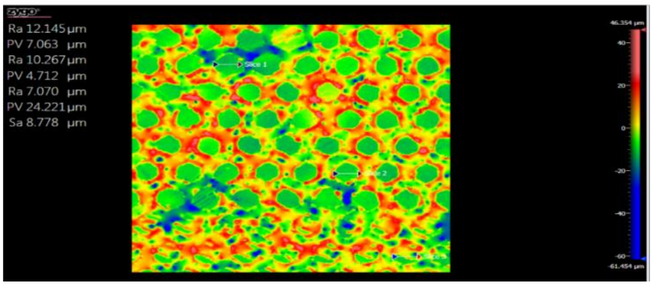

Figure 12. Flatness deviation after texturing - Arbofill Fichte: 4x_H

Figure 13. Roughness value Ra for three reference lines - Arbofill Fichte: 4x_H, on geometric shape

In Figure 14, three sets of data and graphs related to the geometry and measured distances for Arbofill Fichte material with a hexagonal lattice-like structure (similar to a honeycomb-like structure) can be observed. Each of the three sections is accompanied by a graph and information related to the distances measured in the X and Y directions. Analyzing comparatively the data presented in Figure 14, it can be stated that:

√ X axis. Section 1 shows the largest initial distance on the X-axis (72.80 µm), indicating a considerable opening of the structure in the horizontal direction. Section 2 shows significant compression, with a distance of 57.70 µm, suggesting a reduction in the X-axis opening. Section 3 shows considerable extension along the X-axis, at 78.15 µm, indicating high variability along the X-axis, with a very open structure in this section.

√ Yaxis. Section 1 shows maximum Y-axis extension at 26.51 µm, indicating a vertically extended structure. Section 2 has a compression on the Y-axis, with 20.45 µm, suggesting a reduction of the extension in this direction. Section 3 continues the trend of compression on the Y-axis, with 19.66 µm, indicating a more compact structure on this axis.

In conclusion, in terms of the four-pass relining and hexagonal geometry, it is possible to observe that on the X-axis, there is significant variation between sections, with compression in section 2, but maximum extension in section 3. On the Y-axis, a general trend of compression between sections can be observed, with section 1 being the most extended, followed by a decrease in the spans in sections 2 and 3.

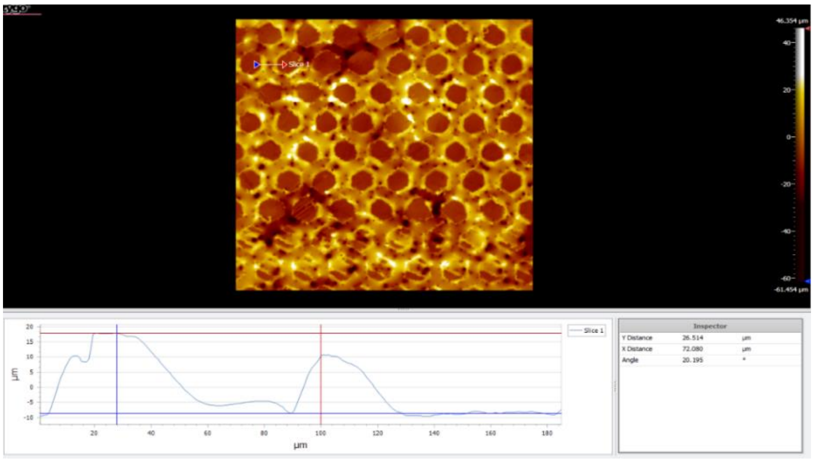

Inspector		
Y Distance	26.514	µm
X Distance	72.080	µm
Angle	20.195	°

Inspector slice 1

Y Distance = 26.51 µm

X Distance = 72.80 µm

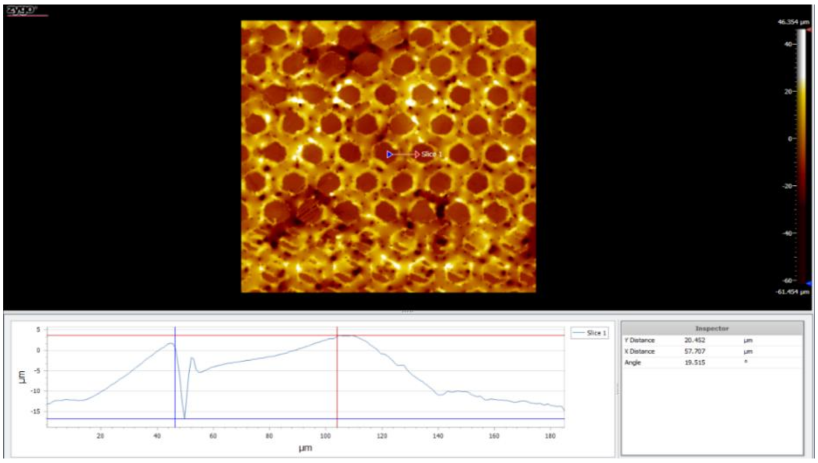

Inspector		
Y Distance	20.452	µm
X Distance	57.707	µm
Angle	19.515	°

Inspector slice 2

Y Distance = 20.45 µm

X Distance= 57.70 µm

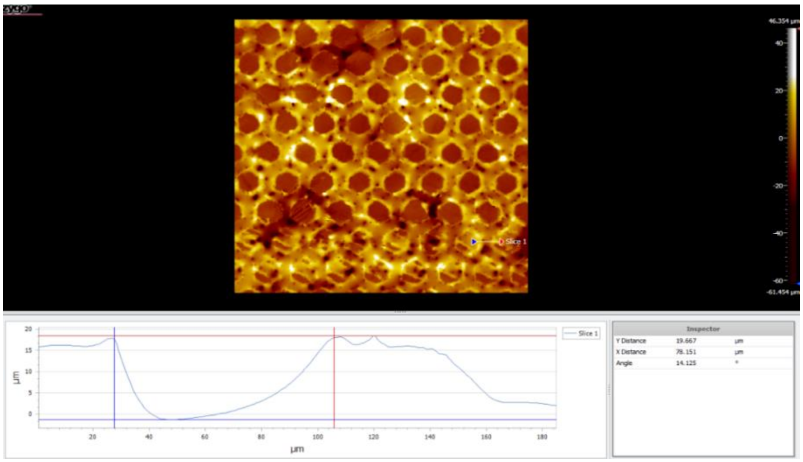

Inspector slice 3

Y Distance = 19.66 µm

X Distance = 78.15 µm

Figure 14. Interstice value for three reference lines – Arbofill Fichte: 4x_H, on the geometric shape.

In the case of the hexagonal texture obtained by 6 passes, shown in in Figure 15, the largest distance between the lowest and the highest peak (PV_Peak and Valley) for the three sections considered, and in Table 6 the corresponding statistical data are presented. More, the mean value for PV is 69.16±25.58 µm and 8.352±1.406 µm for RMS.

Table 6. Statistical data for Arbofill Fichte: 6x_H.

Nr.crt.	Reference line	PV (µm)	RMS (µm)
1	Slice 1	77.68	9.961
2	Slice 2	40.40	6.887
3	Slice 3	89.40	8.478
4	Mean	69.16	8.352
5	Standard deviation	25.58	1.406
6	Range	49.00	2.804
7	3 Sigma	76.75	4.219

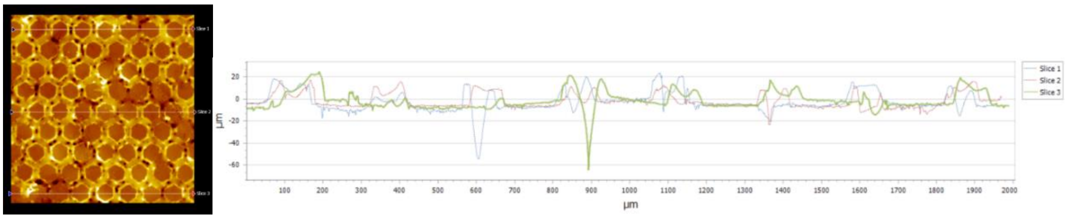

Figure 15. Maximum PV value from the analysis of the three sections - Arbofill Fichte: 6x_H, on the geometric shape.

The flatness deviation after texturing is shown in Figure 16 with a value of 7.828 µm according to ISO Flatness. Figure 17 shows the roughness values Ra for the three reference lines chosen, which correspond only to the hexagonal surfaces obtained without taking into account the distance between hexagons. Thus, the Sa obtained had the value of 7.175 µm, with the highest value of Ra=8.186 µm and PV=14.79 µm both in case of slice 2.

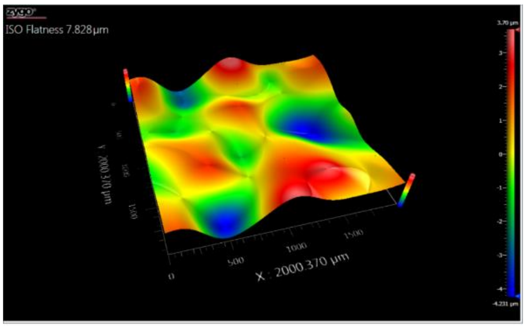

Figure 16. Flatness deviation after texturing - Arbofill Fichte: 6x_H

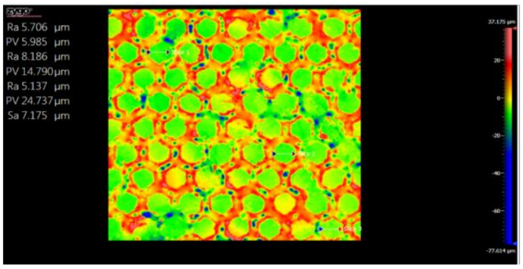
Ra 5.706 µm
PV 5.985 µm
Ra 8.186 µm
PV 14.790µm
Ra 5.137 µm
PV 24.737µm
Sa 7.175 µm

Figure 17. Roughness value Ra for three reference lines - Arbofill Fichte: 6x_H, on the geometric shape

Analyzing the data presented in Figure 18, it is possible to state that:

-Xaxis. Section 1 has a distance of 59.85 µm, suggesting a moderate opening of the structure on this axis. Section 2 shows significant compression, with a distance of 55.99 µm, indicating a reduction in the opening on the horizontal axis. Section 3 has the largest enlargement on the X-axis, at 67.36 µm, indicating a significant variability of the structure.

-Yaxis. On the Y-axis, the distances are fairly constant between the three sections: 23.45 µm, 23.07 µm and 23.25 µm, suggesting a very stable structure on this axis. Vertical compression and extension are minimal, indicating a uniformity in the structure.

In conclusion, with respect to the six-pass relining and hexagonal geometry, it is possible to observe that the X-axis shows a high variability between sections, with a maximum compression in section 2 and a maximum extension in section 3. This indicates a significant variability on the horizontal axis as a function of the number of passes. The Y-axis remains constant in all sections, which indicates excellent stability on the vertical axis with minimal variation between passes.

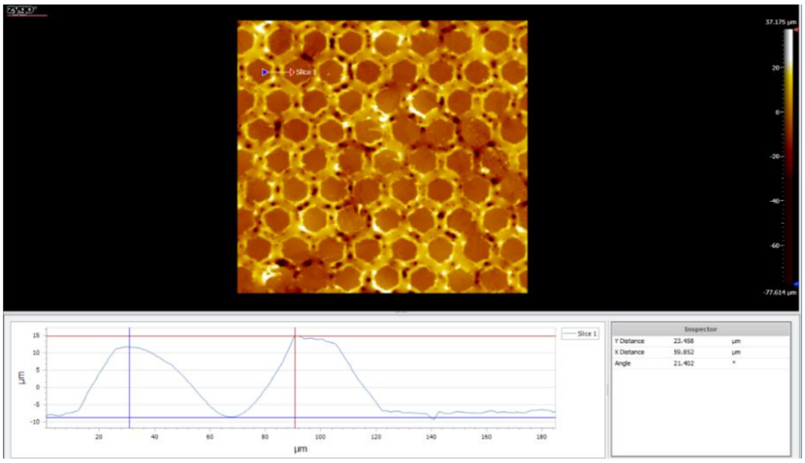

Y Distance	23.458	µm
X Distance	59.852	µm
Angle	21.402	°

Inspector slice 1

Y Distance = 23.45 µm

X Distance = 59.85 µm

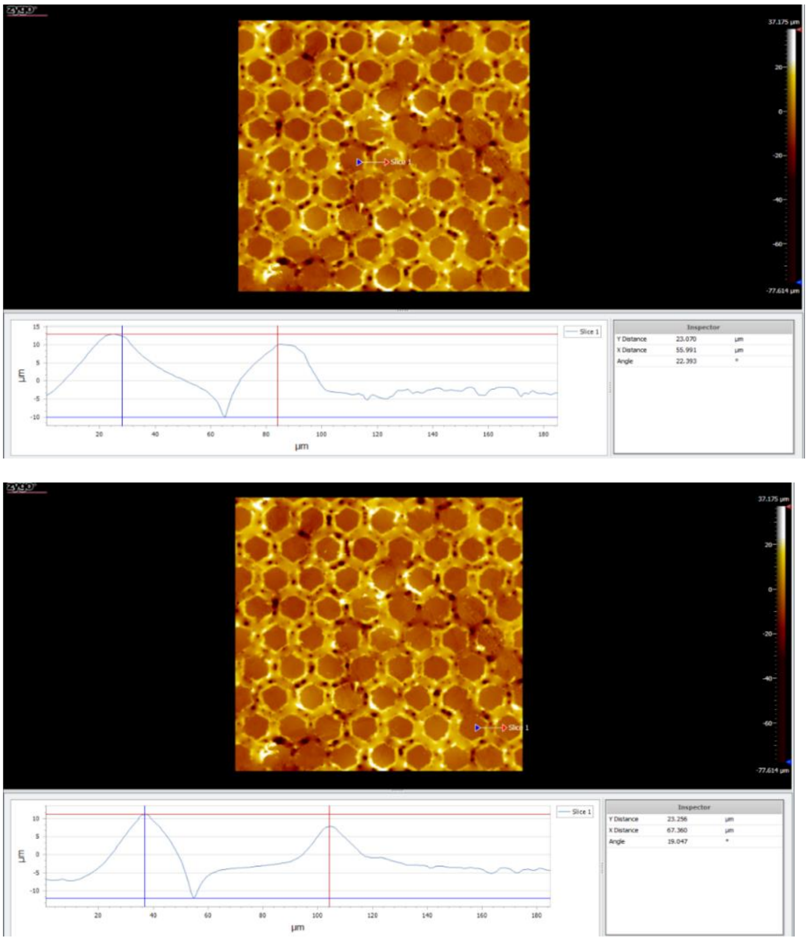

Inspector		
Y Distance	23.070	µm
X Distance	55.991	µm
Angle	22.393	°

Inspector		
Y Distance	23.256	µm
X Distance	67.360	µm
Angle	19.047	°

Inspector slice 2

Y Distance = 23.07 µm

X Distance= 55.99 µm

Inspector slice 3

Y Distance = 23.25 µm

X Distance = 67.36 µm

Figure 18. Gap value for three reference lines - Arbofill Fichte: 6x_H, on geometric shape.

3.5.2. Comparative Analysis Between the Two Processing Models 4x_H/6x_H

Comparatively analyzing both laser texturing passes 4x and 6x, it can be stated that:

-In the case of the X-axis, in 4 passes (4x), the X-axis distances varied between 57.70 µm and 78.15 µm, suggesting a large extension of the structure along this axis in certain sections. Increasing the number of passes to 6 (6x), causes the distances to vary between 55.09 µm and 67.36 µm, with greater compression in the X-axis compared to 4x, but with maximum expansion in section 3, indicating high variability in this case.

-In the case of the Y-axis, at 4 passes (4x), the distances varied between 19.66 µm and 26.51 µm, indicating a gradual compression in the vertical axis, with significant variation between sections. At 6 passes (6x), the distances were approximately constant between 23.05 µm and 23.45 µm, suggesting superior stability on the Y(depth) axis, with no significant variation between sections.

This analysis indicates that the 6 passes material is more uniform on the Y(depth) axis, while the 4 passes material undergoes more changes on the vertical axis. The X-axis structure is variable in both cases, but with higher compression at 6 passes.

3.5.3. Topographic Analysis in the Case of Arbofill Fichte Material with a Square Texture

In the case of the Arbofill Fichte material with a square texture obtained through 4 passes, Figure 19 shows the largest distance between the lowest and the highest peak (PV_Peak to Valley) for the three sections considered, and in Table 7 corresponding statistical data are presented. The PV mean value was 44.75±7.17 µm and RMS value was 6.416±0.814 µm.

Table 7. Statistical data in the case of the material Arbofill Fichte: 4x_S**.**

Nr.crt.	Reference line	PV (µm)	RMS (µm)
1	Slice 1	39.75	5.784
2	Slice 2	52.97	7.334
3	Slice 3	41.54	6.130
4	Mean	44.75	6.416
5	Standard deviation	7.17	0.814
6	Range	13.22	1.550
7	3 Sigma	21.52	2.441

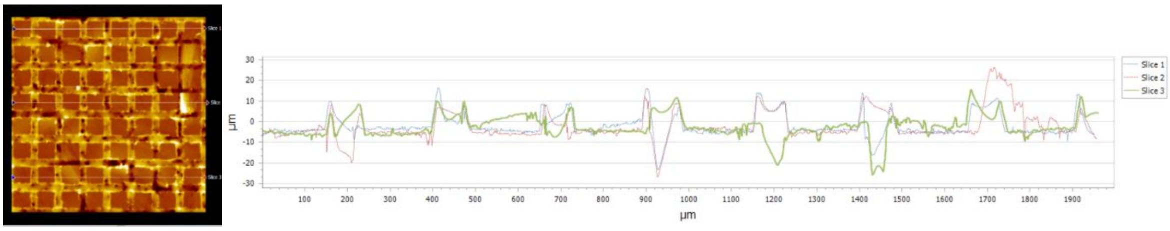

Figure 19. The maximum PV value from the analysis of the three sections – Arbofill Fichte: 4x_S, on the geometric shape.

The flatness deviation after texturing is shown in Figure 20 with a value of 4.261 µm according to ISO Flatness. Figure 21 shows the roughness values Ra for the three reference lines chosen (5.551 µm as mean value), which correspond only to the square surfaces obtained without taking into account the distance between squares and Sa value of 6.335 µm

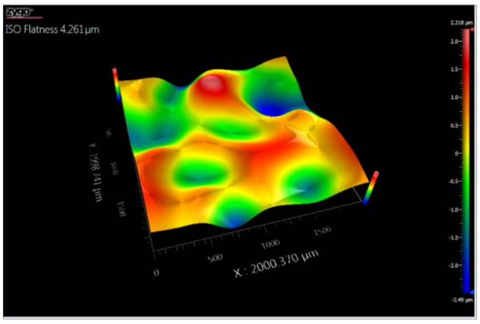

Figure 20. Flatness deviation after texturing – Arbofill Fichte: 4x_S

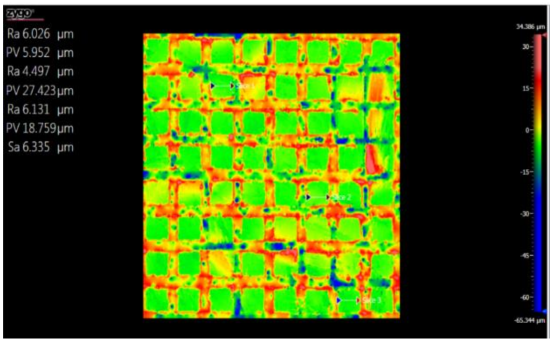

Figure 21. Roughness value Ra for three reference reference lines – Arbofill Fichte: 4x_S, on the geometric shape

Figure 22 shows three sets of data and graphs related to the geometry and distances measured for the Arbofill Fichte material with a square texture. Each of the three sections is accompanied by a graph and information related to the distances measured in the X and Y directions. Comparatively analyzing the data presented in Figure 22, the following can be stated: along the X Axis, section 1 presents a distance of 56.20µm, indicating a moderate expansion in the X axis, section 2 has a slightly higher value of 59.85µm, suggesting further extension of the structure in this axis, and section 3 shows a significant compression in the X axis, with 43.34µm, the smallest distance between all sections; along the Y-axis section 1 shows a spacing of 21.50µm, indicating moderate Y-axis extension, section 2 has a much larger extension of 44.92µm, suggesting maximum vertical extension in this section and section 3 shows a value almost identical to section 1, of 21.36µm, indicating a compression compared to section 2.

Basically, it can be stated that in the case of this square geometry, both axes (longitudinal X and depth Y) behave differently. The X-axis shows significant compression in section 3, while sections 1 and 2 show relatively stable expansion, with section 2 being slightly more extended. The Y-axis shows a maximum extension in section 2, suggesting significant variability on this axis, while sections 1 and 3 show moderate and similar compression on the vertical axis.

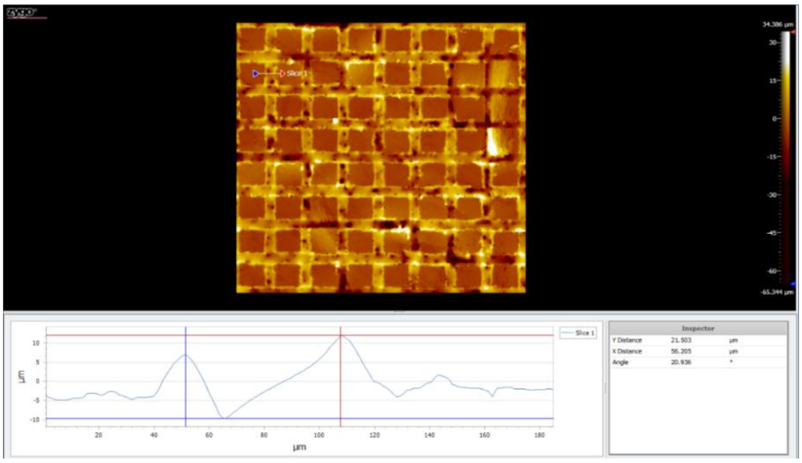

Inspector		
Y Distance	21.503	µm
X Distance	56.205	µm
Angle	20.936	°

Inspector slice 1

Y Distance = 21.50 µm

X Distance = 56.20 µm

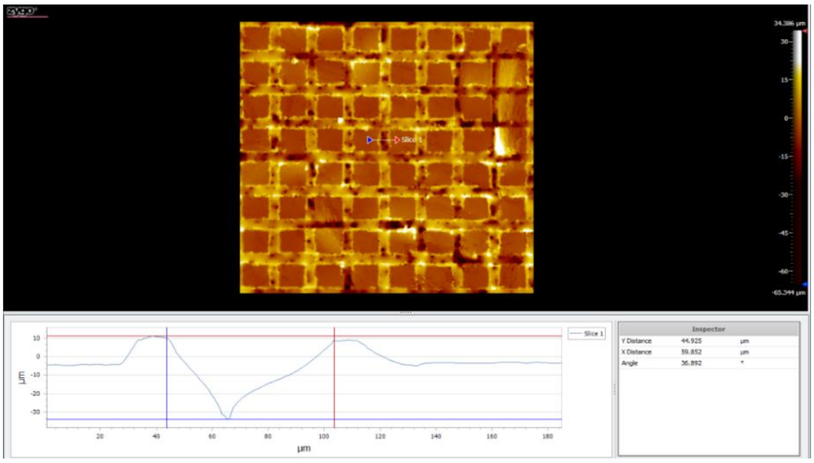

Inspector		
Y Distance	44.925	µm
X Distance	59.852	µm
Angle	36.892	°

Inspector slice 2

Y Distance = 44.92 µm

X Distance= 59.85 µm

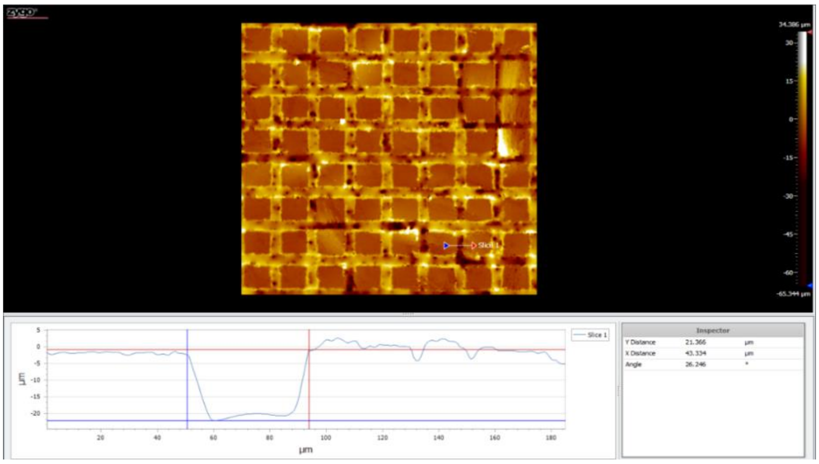

Inspector		
Y Distance	21.366	µm
X Distance	43.334	µm
Angle	26.246	°

Inspector slice 3

Y Distance = 21.36 µm

X Distance = 43.33 µm

Figure 22. PV value for three reference lines – Arbofill Fichte: 4x_S, on the geometric form.

In the case of the Arbofill Fichte material with a square texture obtained through 6 passes, Figure 23 shows the largest distance between the lowest and the highest peak (PV, Peak to Valley) for the three sections considered, and in Table 8 corresponding statistical data are presented. Mean value of PV is 41.82±4.34 µm and 7.491±0.562 µm.

Table 8. Statistical data in the case of the material Arbofill Fichte: 6x_S**.**

Nr.crt.	Reference line	PV (µm)	RMS (µm)
1	Slice 1	42.88	6.953
2	Slice 2	37.04	7.446
3	Slice 3	45.54	8.074
4	Mean	41.82	7.491
5	Standard deviation	4.34	0.562
6	Range	8.49	1.121
7	3 Sigma	13.03	1.686

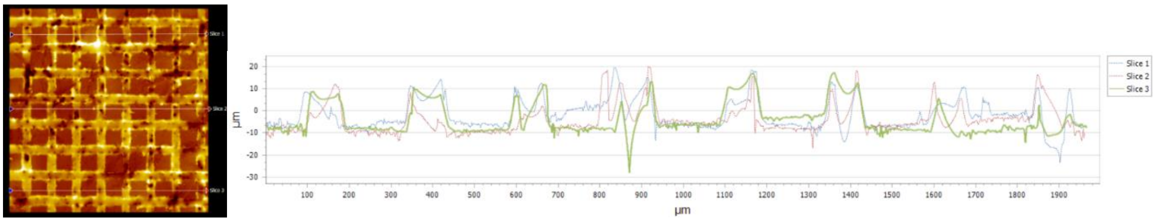

Figure 23. The maximum PV value from the analysis of the three sections – Arbofill Fichte: 6x_S, on the geometric shape.

The flatness deviation after texturing is shown in Figure 24 with a value of 6.892µm according to ISO Flatness. Figure 25 shows the values of the roughness Ra for the three chosen reference lines (minimum value 6.841 µm and maximum 8.245 µm), which correspond only to the square surfaces obtained (7.643 µm) without taking into account the distance between them.

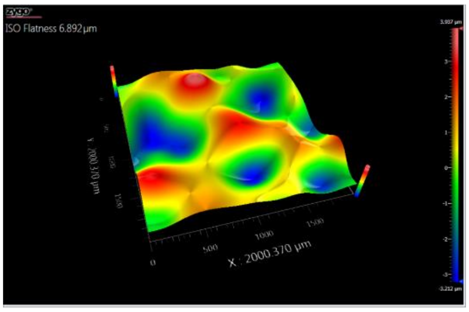

Figure 24. Flatness deviation after texturing – Arbofill Fichte: 6x_S

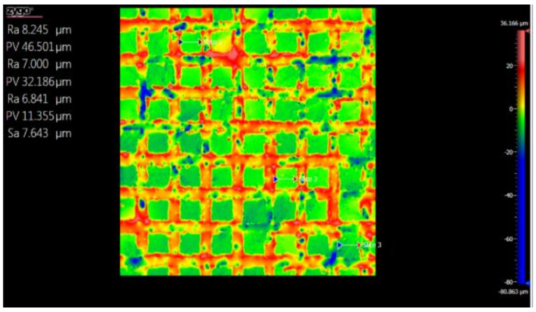

Figure 25. Roughness value Ra for three reference lines – Arbofill Fichte: 6x_S, on the geometric form

Comparatively analyzing the data presented in Figure 26, the following aspects can be mentioned: along the X axis, section 1 shows a distance of 57.70µm, which indicates a moderate expansion on the X axis, section 2 has a distance of 71.43µm, suggesting an expansion maximum of the structure in the horizontal direction and section 3 shows a slight compression, with a distance of 59.63µm, indicating a reduction of the X-axis extension; along the Y-axis, section 1 shows a moderate Y-axis extension of 24.91µm, section 2 shows a maximum Y-axis extension of 41.48µm, suggesting significant variability along this axis, and section 3 shows a pronounced compression, by 17.23µm, indicating a considerable reduction in the vertical axis extension.

Comparatively, the X-axis shows maximum expansion in section 2, with moderate compression in sections 1 and 3. This suggests considerable variability on the horizontal axis. The Y-axis shows significant expansion in section 2, followed by considerable compression in section 3, indicating an instability of the structure on the vertical axis.

doi:10.20944/preprints202412.0943.v1

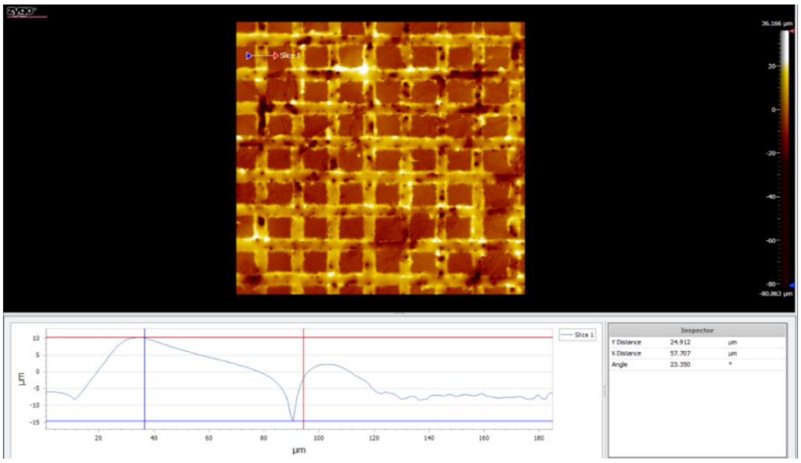

Inspector		
Y Distance	24.912	µm
X Distance	57.707	µm
Angle	23.350	°

Inspector slice 1

Y Distance = 24.91 µm

X Distance = 57.70 µm

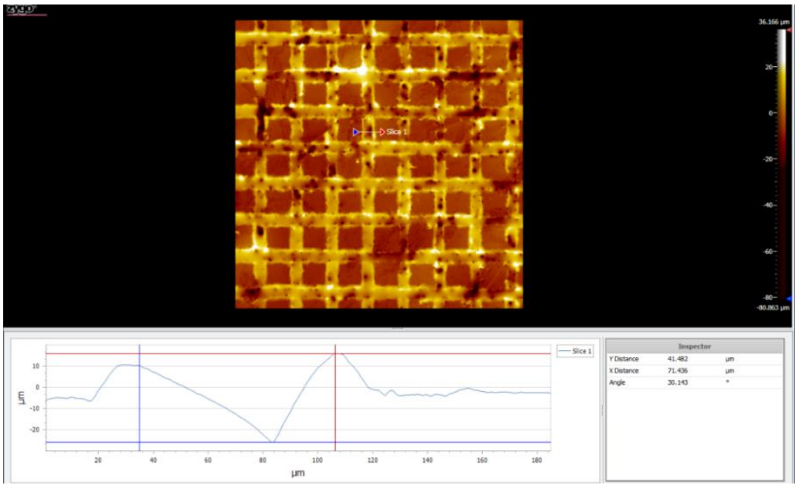

Inspector		
Y Distance	41.482	µm
X Distance	71.436	µm
Angle	30.143	°

Inspector slice 2

Y Distance = 41.48 µm

X Distance= 71.43 µm

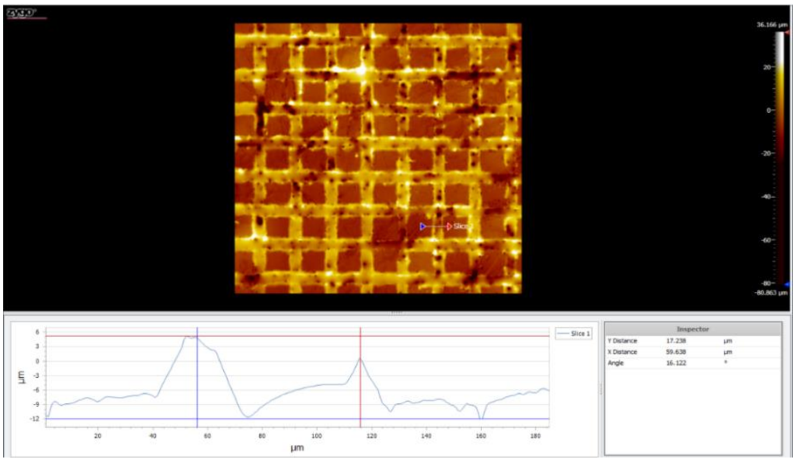

Inspector		
Y Distance	17.238	µm
X Distance	59.638	µm
Angle	16.122	°

Inspector slice 3

Y Distance = 17.23 µm

X Distance = 59.63 µm

Figure 26. Interstices value for three reference lines – Arbofill Fichte: 6x_S, on the geometric shape.

3.5.4. Comparative Analysis of the Two Types of Processing 4x_S and 6x_S

Along the X-axis, at 4 passes (4x), the distances ranged between 43.34µm and 59.85µm, suggesting a relatively stable extension with significant compression only in section 3, and at 6 passes (6x), the distances ranged from 57.70µm and 71.43µm, indicating greater expansion in the X-axis at the higher number of passes, but also moderate compression in section 3.

Along the Y-axis, in the 4-pass (4x) situation, the distances varied between 21.36µm and 44.92µm, with a maximum expansion in section 2 and a compression in sections 1 and 3, and at 6 passes (6x), distances ranged between 17.23µm and 41.48µm, showing a similar variability to 4 passes, but with a more pronounced compression in section 3.

In conclusion, it can be stated that the 6-pass machining (6x) shows higher X-axis extensions, but also significant variability, with a compression in section 3. The 4-pass (4x) square geometry is relatively stable in the X-axis, but undergoes greater compression in section 3 on the Y-axis. On the Y-axis, the geometry obtained after the 6 passes shows a more pronounced compression, while at 4 passes we have a more uniform expansion between the sections. These differences suggest that the number of passes significantly influences the variability and expansion on the X and Y axes, with 6 passes resulting in greater expansions, but also more obvious compressions in certain areas.

3.5.5. Comparison of Hexagonal and Square Geometry 4 and 6 Passes

Hexagonal geometry (4x and 6x) along the X-axis. In 4-pass (4x) machining, the X-axis distances for the hexagonal geometry ranged from 45.19µm to 46.70µm, indicating a relatively uniform spread in the horizontal direction, with variations minimums between sections. At 6 passes (6x), the X-axis distances ranged from 40.39µm to 46.70µm, suggesting more pronounced compression along this axis, but with moderate and uniform expansion.

Square geometry (4x and 6x) along the X-axis. At 4 passes (4x), the X-axis distances for the square geometry ranged from 43.34µm to 59.85µm, indicating significant extension in the horizontal direction, with an obvious compression in section 3. At 6 passes (6x), the X-axis distances ranged from 57.70µm to 71.43µm, indicating further X-axis expansion, especially in section 2, but also moderate compression in section 3.

Hexagonal geometry (4x and 6x) along the Y-axis. In 4 passes (4x), the Y-axis distances ranged from 2.66µm to 7.78µm, indicating considerable compression in the vertical axis, with greater variability between sections. At 6 passes (6x), Y-axis distances ranged from 3.92µm to 9.79µm, indicating a slight increase in extension over 4 passes, but compression in this axis remains significant.

Square geometry (4x and 6x) along the Y-axis. In 4 passes (4x), the Y-axis distances ranged from 21.36µm to 44.92µm, indicating maximum expansion in section 2 and moderate compression in sections 1 and 3. At 6 passes (6x), the Y-axis distances ranged from 17.23µm to 41.48µm, with a pronounced compression in section 3 but a significant expansion in section 2.

5. Conclusions

The wettability test showed the weak hydrophobic character of the surface (the contact angle close to 90°) regardless of the type of texture obtained.

Surface modification by LST induced a change in the wear behaviour of the base material. For all samples, an increase of COF values was recorded and it was found that the textured pattern was removed during the wear test, under the proposed conditions.

After the degradation test, an increase in weight was observed for all samples. Generally, an increase in weight of polymer materials after a degradation test could indicate incomplete degradation; if the degradation process is not fully completed, residues from partially degraded polymer molecules may remain, contributing to the weight increase. However, based on the microscopic observation of all samples after the degradation test, no degradation products were visible.

On the topography side, the Arbofill Fichte shows a higher Y-axis stability in both geometries, suggesting a better resistance to vertical compression (subsidence), especially at 6 passes. Arbofill Fichte is stable and uniform in both geometries and at both numbers of texturing passes, giving a more constant X-axis expansion and better controlled Y-axis compression. This makes it easier to predict behavior under certain processing regimes. In terms of geometry, the hexagonal geometry is more stable and uniform in extension on both axes, especially on the X-axis, where variations are minimal. On the Y-axis, the hexagonal geometry undergoes more significant compression (better depth) but is less variable between sections, while the square geometry is more extended on the X-axis at both types of passes and undergoes greater variations between sections, especially on the Y-axis, where the extension may be maximum in some sections and compressed in others. The square geometry is more sensitive to the number of passes, with larger variations at 6 passes, but also with pronounced compression in some sections.

Author Contributions: Conceptualization, D.N. and M.A.; methodology, P.D.R; introduction, D.M.; microscopy, wettability and degradation tests, O.B.; wear and COF tests, A.W.; formal analysis, materials and methods, S-N.M.; topography tests, C.T.; writing—original draft preparation, D.N.; project administration, D.N. and M.A.; funding acquisition, D.N. All authors have read and agreed to the published version of the manuscript.

Funding: This research was funded by "Gheorghe Asachi" Technical University of Iasi, Bd. Dimitrie, Mangeron, no. 53A, 700050 Iasi, Romania, under funding number432/09.01.2023.

Data Availability Statement: Not applicable.

Conflicts of Interest: The authors declare no conflict of interest.

References

1. Li, D.; Chen, X.; Guo, C.; Tao, J.; Tian, C.; Deng, Y.; Zhang, W. Micro surface texturing of alumina ceramic with nanosecond laser. Procedia Eng. 2017, 174, 370–376.
2. Xing, Y.; Deng, J.; Feng, X.; Yu, S. Effect of laser surface texturing on Si3N4/TiC ceramic sliding against steel under dry friction. Mater. Design (1980–2015) 2013, 52, 34–45.
3. Šugár, P.; Šugárová, J.; Frnčík, M. Laser surface texturing of tool steel: Textured surfaces quality evaluation. Open Eng. 2016, 6, 90–97.
4. Tripathi, K.; Gyawali, G.; Joshi, B.; Amanov, A.; Wohn, S. Improved tribological behavior of grey cast Iron Under low and high viscous lubricants by laser surface texturing. Mater. Perform. Charact. 2017, 6, 24–41.
5. Riveiro, A.; Maçon, A.L.; del Val, J.; Comesaña, R.; Pou, J. Laser surface texturing of polymers for biomedical applications. Front. Phys. 2018, 6, 16.
6. Ezhilmaran, V.; Vasa, N.J.; Vijayaraghavan, L. Investigation on generation of laser assisted dimples on piston ring surface and influence of dimple parameters on friction. Surf. Coat. Technol. 2018, 335, 314–326.
7. Liang, L.; Yuan, J.; Li, X.; Yang, F.; Jiang, L. Wear behavior of the micro-grooved texture on WC-Ni3Al cermet prepared by laser surface texturing. Int. J. Refract. Met. Hard Mater. 2018, 72, 211–222.
8. Ishwer Shivakoti, Golam Kibria, Robert Cep, Bal Bahadur Pradhan, Ashis Sharma, Laser Surface Texturing for Biomedical Applications: A Review, Coatings 2021, 11(2), 124; https://doi.org/10.3390/coatings11020124
9. White, N.; Eder, K.; Byrnes, J.; Cairney, J.M.; McCarroll, I.E. Laser ablation sample preparation for atom probe tomography and transmission electron microscopy. Ultramicroscopy 2020, 220, 113161.
10. Antonio Riveiro, Anthony L. B. Maçon, Jesus del Val, Rafael Comesaña, Juan Pou, Laser Surface Texturing of Polymers for Biomedical Applications, Front. Phys., Sec. Optics and Photonics, Volume 6, https://doi.org/10.3389/fphy.2018.00016
11. Tomanik, M.; Kobielarz, M.; Filipiak, J.; Szymonowicz, M.; Rusak, A.; Mroczkowska, K.; Antończak, A.; Pezowicz, C. Laser Texturing as a Way of Influencing the Micromechanical and Biological Properties of the Poly (L-Lactide) Surface. Materials 2020, 13, 3786.
12. Riveiro, A.; Soto, R.; Del Val, J.; Comesaña, R.; Boutinguiza, M.; Quintero, F.; Lusquiños, F.; Pou, J. Texturing of polypropylene (PP) with nanosecond lasers. Appl. Surf. Sci. 2016, 374, 379–386.
13. V. Dinca, P. Alloncle, P. Delaporte, V. Ion, L. Rusen, M. Filipescu, C. Mustaciosu, C. Luculescu, M. Dinescu, Excimer laser texturing of natural composite polymer surfaces for studying cell-to-substrate specific response, Applied Surface Science, 352, 2015, 82-90, https://doi.org/10.1016/j.apsusc.2015.02.141.
14. Koufaki, N.; Ranella, A.; Aifantis, K.E.; Barberoglou, M.; Psycharakis, S.; Fotakis, C.; Stratakis, E. Controlling cell adhesion via replication of laser micro/nano-textured surfaces on polymers. Biofabrication 2011, 3, 045004.
15. Yeong, W.Y.; Yu, H.; Lim, K.P.; Ng, K.L.; Boey, Y.C.; Subbu, V.S.; Tan, L.P. Multiscale topological guidance for cell alignment via direct laser writing on biodegradable polymer. Tissue Eng. Part C Methods 2010, 16, 1011–1021.
16. Waugh, D.; Lawrence, J. Laser surface processing of polymers for biomedical applications. In Laser-Assisted Fabrication of Materials; Springer: Berlin/Heidelberg, Germany, 2013; pp. 275–318.
17. Jagur-Grodzinski J. Polymers for tissue engineering, medical devices, and regenerative medicine. Concise general review of recent studies. Polym Adv Technol. (2006) 17:395–418. doi: 10.1002/pat.729

18. Kohane DS, Langer R, Langer R. Polymeric biomaterials in tissue engineering. Pediatr Res. (2008) 63:487–91. doi: 10.1203/01.pdr.0000305937.26105.e7
19. Teo AJT, Mishra A, Park I, Kim YJ, Park WT, Yoon YJ. Polymeric biomaterials for medical implants and devices. ACS Biomater Sci Eng. (2016) 2:454–72. doi: 10.1021/acsbiomaterials.5b00429
20. Abu Bakar MS, Cheng MHW, Tang SM, Yu SC, Liao K, Tan CT, et al. Tensile properties, tension–tension fatigue and biological response of polyetheretherketone–hydroxyapatite composites for load-bearing orthopedic implants. Biomaterials (2003) 24:2245–50. doi: 10.1016/S0142-9612(03)00028-0
21. Godara A, Raabe D, Green S. The influence of sterilization processes on the micromechanical properties of carbon fiber-reinforced PEEK composites for bone implant applications. Acta Biomater. (2007) 3:209–20. doi: 10.1016/j.actbio.2006.11.005
22. Riveiro A, Soto R, Comesa-a R, Boutinguiza M, Del V, Quintero F, et al. Laser surface modification of PEEK. Appl Surf Sci. (2012) 258:9437–42. doi: 10.1016/j.apsusc.2012.01.154
23. Zheng Y, Xiong C, Wang Z, Li X, Zhang L. A combination of CO_2 laser and plasma surface modification of poly(etheretherketone) to enhance osteoblast response. Appl Surf Sci. (2015) 344:79–88. doi: 10.1016/j.apsusc.2015.03.113
24. Wilson A, Jones I, Salamat-Zadeh F, Watts JF. Laser surface modification of poly(etheretherketone) to enhance surface free energy, wettability and adhesion. Int J Adhes Adhes. (2015) 62:69–77. doi: 10.1016/j.ijadhadh.2015.06.005
25. Lorusso A, Nassisi V, Paladini F, Torrisi L, Visco AM, Campo N. Comparison of the laser effects induced on ultra-high-molecular-weight polyethylene. Radiat Eff Defects Solids (2008) 163:435–40. doi: 10.1080/10420150701778155
26. Riveiro A, Soto R, del Val J, Comesa-a R, Boutinguiza M, Quintero F, et al. Laser surface modification of ultra-high-molecular-weight polyethylene (UHMWPE) for biomedical applications. Appl Surf Sci. (2014) 302:236–42. doi: 10.1016/j.apsusc.2014.02.130
27. Himma NF, Anisah S, Prasetya N, Wenten IG. Advances in preparation, modification, and application of polypropylene membrane. J Polym Eng. (2016) 36:329–62. doi: 10.1515/polyeng-2015-0112
28. Wissemborski R, Klein R. Welding and marking of plastics with lasers. Laser Tech J. (2010) 7:19–22. doi: 10.1002/latj.201090070
29. Stanford CM. Surface modifications of dental implants. Aust Dent J. (2008) 53:S26–33. doi: 10.1111/j.1834-7819.2008.00038.x
30. Murahara M, Okoshi M. Photochemical surface modification of polypropylene for adhesion enhancement by using an excimer laser. J Adhes Sci Technol. (1995) 9:1593–9. doi: 10.1163/156856195X00220
31. Deshpande S, Munoli A. Long-term results of high-density porous polyethylene implants in facial skeletal augmentation: an Indian perspective. Indian J Plast Surg Off Publ Assoc Plast Surg India (2010) 43:34–9. doi: 10.4103/0970-0358.63955
32. Okoshi M, Inoue N. Microfabrication of polyethylene using femtosecond Ti:sapphire laser and nanosecond ArF laser. Jpn J Appl Phys. (2003) 42:5642. doi: 10.1143/JJAP.42.5642
33. Blanchemain N, Chai F, Bacquet M, Gengembre L, Traisnel M, Setti Y, et al. Improvement of biological response of YAG laser irradiated polyethylene. J Mater Chem. (2007) 17:4041–9. doi: 10.1039/b708250a
34. Okoshi M, Inoue N. Laser ablation of polymers using 395 nm and 790 nm femtosecond lasers. Appl Phys Mater Sci Process. (2004) 79:841–4. doi: 10.1007/s00339-004-2815-7
35. Ahad IU, Budner B, Korczyc B, Fiedorowicz H, Bartnik A, Kostecki J, et al. Polycarbonate polymer surface modification by extreme ultraviolet (EUV) radiation. Acta Phys Pol A (2014) 125:924–8. doi: 10.12693/APhysPolA.125.924
36. Viville P, Beauvois S, Lambin G, Lazzaroni R, Brédas JL, Kolev K, et al. Excimer laser-induced surface modifications of biocompatible polymer blends. Appl Surf Sci. (1996) 96:558–562. doi: 10.1016/0169-4332(95)00530-7
37. Ahad IU, Butruk B, Ayele M, Budner B, Bartnik A, Fiedorowicz H, et al. Extreme ultraviolet (EUV) surface modification of polytetrafluoroethylene (PTFE) for control of biocompatibility. Nucl Instrum Methods Phys Res Sect B Beam Interact Mater Atoms (2015) 364:98–107. doi: 10.1016/j.nimb.2015.08.093
38. Waugh DG, Lawrence J, Morgan DJ, Thomas CL. Interaction of CO_2 laser-modified nylon with osteoblast cells in relation to wettability. Mater Sci Eng C (2009) 29:2514–24. doi: 10.1016/j.msec.2009.07.020
39. Günther D, Scharnweber D, Hess R, Wolf-Brandstetter C, Grosse Holthaus M, Lasagni AF. High precision patterning of biomaterials using the direct laser interference patterning technology. In: Vilar R, editor. Laser

Surface Modification of Biomaterials. Cambridge, MA: Woodhead Publishing (2016). doi: 10.1016/B978-0-08-100883-6.00001-0

40. Yasaka K., Koseki Y., Yoshinaka K., Miyake K., Effects of Surface Texture on Soft-Materials for Medical Applications, Tribology online, 2016, 11(2), https://doi.org/10.2474/trol.11.288
41. Ikeuchi, K., Takii, T., Norikane, H., Tomita, N., Ohsumi, T., Uyama, Y. and Ikada, Y., "Water Lubrication of Polyurethane Grafted with Dimethylacrylamide for Medical Use," Wear, 161, 1-2, 1993, 179-185, https://doi.org/10.1016/0043-1648(93)90467-Z
42. Shivakoti I., Kibria G., Cep R., Pradhan B.B., Sharma A., Laser surface texturing for biomedical applications: A review, Coatings 2021, 11(2), 124; https://doi.org/10.3390/coatings11020124
43. Mirzadeh, H.; Katbab, A.A.; Burford, R.P. CO2-laser graft copolymerization of HEMA and NVP onto ethylene-propylene rubber (EPR) as biomaterial-(III). Radiat. Phys. Chem. 1995, 46, 859–862
44. Koufaki, N.; Ranella, A.; Aifantis, K.E.; Barberoglou, M.; Psycharakis, S.; Fotakis, C.; Stratakis, E. Controlling cell adhesion via replication of laser micro/nano-textured surfaces on polymers. Biofabrication 2011, 3, 045004
45. Evangelista I., Wencel D., Beguin S., Zhang N., Gilchrist M.D., Influence of Surface Texturing on the Dry Tribological Properties of Polymers in Medical Devices, Polymers (Basel), 15(13): 2858, doi: 10.3390/polym15132858
46. Affatato S., Brando D. Wear of Orthopaedic Implants and Artificial Joints. Woodhead Publishing; Sawston, UK: 2013. Introduction to wear phenomena of orthopaedic implants; pp. 3–26.
47. Ching H.A., Choudhury D., Nine M.J., Abu Osman N.A. Effects of surface coating on reducing friction and wear of orthopaedic implants. Sci. Technol. Adv. Mater. 2014;15:014402. doi: 10.1088/1468-6996/15/1/014402
48. Howard J.J. Balancing innovation and medical device regulation: The case of modern metal-on-metal hip replacements. Med. Devices. 2016;9:267–275. doi: 10.2147/MDER.S113067
49. Bialas O., Lis M., Wozniak A., Adamiak M., Laser Superficial Fusion of Gold Nanoparticles with PEEK Polymer for Cardiovascular Application, Materials 2021, 14(4), 971; https://doi.org/10.3390/ma14040971.
50. Nedelcu D., Plavanescu S., Puiu E., Impact resistance of "liquid wood", Advanced Materials Research 1036, 13-17
51. Mazurchevici S., Quadrini F., Nedelcu D., The liquid wood heat flow and material properties as a function of temperature, Materials Research Express 5 (3), 035303
52. Broitman E., Nedelcu D., Mazurchevici S., Glenat H., Grillo S., Tribological and nanomechanical behavior of liquid wood, Journal of Tribology 141 (2), 022001
53. Nedelcu D., Investigation on microstructure and mechanical properties of samples obtained by injection from Arbofill, Composites Part B: Engineering 47, 126-129
54. Simona-Nicoleta Mazurchevici, Dorin Vaideanu, Doreen Rapp, Cristian-Dragos Varganici, Constantin Cărăușu, Mihai Boca, Dumitru Nedelcu, Dynamic mechanical analysis and thermal expansion of lignin-based biopolymers, Polymers 13 (17), 2953
55. Available online: https://www.tecnaro.de/en/arboblend-arbofill-arboform/verarbeitung/ (accessed on 12 September 2022).
56. D Nedelcu, C Ciofu, NM Lohan, Microindentation and differential scanning calorimetry of "liquid wood", Composites Part B: Engineering 55, 11-15.